Chemistry of *C*-Trimethylsilyl-Substituted Main-Group Heterocarboranes. 7. Reactivity of *closo*-Germa- and *closo*-Plumbacarboranes toward a Bis(bidentate) Lewis Base, 2,2′-Bipyrimidine: Syntheses and Structures of 1- or 1,1′-(2,2′-$C_8H_6N_4$)[*closo*-1-M-2-(Me_3Si)-3-(R)-2,3-$C_2B_4H_4$]$_n$ (*n* = 1, M = Ge; *n* = 2, M = Pb; R = Me_3Si, Me, H)

Narayan S. Hosmane,* Kai-Juan Lu, Upali Siriwardane, and Manjunath S. Shet

Department of Chemistry, Southern Methodist University, Dallas, Texas 75275

Received March 21, 1990

The unbridged germacarborane complexes 1-Ge-(2,2′-$C_8H_6N_4$)-2,3-($SiMe_3$)$_2$-2,3-$C_2B_4H_4$ (I), 1-Ge-(2,2′-$C_8H_6N_4$)-2-($SiMe_3$)-3-(Me)-2,3-$C_2B_4H_4$ (II), and 1-Ge-(2,2′-$C_8H_6N_4$)-2-($SiMe_3$)-3-(H)-2,3-$C_2B_4H_4$ (III) were synthesized, in yields of 78–84%, from reactions involving the corresponding *closo*-germacarborane and 2,2′-bipyrimidine in a respective ratio of 2:1 at room temperature in benzene solution over a period of 7–8 days. The complexes I, II, and III were characterized on the basis of ^1H, ^{11}B, and ^{13}C pulse Fourier transform NMR, IR, and mass spectroscopy. The crystal structure of I with one molecule of cocrystallized 2,2′-bipyrimidine shows that the complex consists of only one distorted germacarborane unit, and a bipyrimidine molecule, which acts unusually as a monodentate ligand, is bonded to the apical Ge atom. This Ge-bound 2,2′-bipyrimidine base is not situated exactly opposite the C–C(cage) bond; rather, it is tilted toward the two basal borons above the C_2B_3 face. The nonbonded contacts between the atoms of I and the cocrystallized 2,2′-bipyrimidine exceed the sum of their van der Waals radii, and consequently, the geometry of the complex was unaffected by the presence of an extra molecule of the ligand in the crystal lattice. Complex I crystallized in the monoclinic space group $P2_1/n$ with a = 7.765 (9) Å, b = 37.69 (6) Å, c = 9.651 (16) Å, β = 101.41 (1)°, V = 2768 (2) Å^3, and Z = 4. Full-matrix least-squares refinements of I converged at R = 0.065 and R_w = 0.077. Although the *closo*-plumbacarboranes form the expected bridged complexes 1,1′-(2,2′-$C_8H_6N_4$)[*closo*-1-Pb-2,3-($SiMe_3$)$_2$-2,3-$C_2B_4H_4$]$_2$ (IV), 1,1′-(2,2′-$C_8H_6N_4$)[*closo*-1-Pb-2-($SiMe_3$)-3-(Me)-2,3-$C_2B_4H_4$]$_2$ (V), and 1,1′-(2,2′-$C_8H_6N_4$)[*closo*-1-Pb-2-($SiMe_3$)-3-(H)-2,3-$C_2B_4H_4$]$_2$ (VI) with 2,2′-bipyrimidine in 48–58% yields, their slow formation is consistent with that of the germacarborane system in which complexation between the heterocarborane and the Lewis base was kinetically controlled. The complexes IV, V, and VI were characterized by ^1H, ^{11}B, and ^{13}C NMR, IR, and mass spectroscopy, and the single-crystal X-ray analyses were performed on two crystal modifications, IVA and IVB, of the complex IV. The calculated density of IVA is greater than that of IVB and is consistent with the crystal packing. The crystal structures show that the molecular geometries of both modifications are identical in that the apical lead is slipped significantly from the centroidal position above the C_2B_3 face in a distorted-pentagonal-bipyramidal geometry. The direct relationship between the crystal packing and the ligand–ligand dihedral angle was also evident in these structures. Complexes IVA and IVB crystallized in the monoclinic space groups $P2_1/n$ and $P2_1/a$ with a = 8.488 (5) and 13.882 (5) Å, b = 24.46 (2) and 9.854 (3) Å, c = 9.540 (7) and 16.104 (8) Å, β = 96.20 (5) and 105.91 (4)°, V = 1969 (2) and 2118.4 (15) Å^3, and Z = 2 and 2, respectively. Full-matrix least-squares refinements of IVA and IVB converged at R = 0.037 and 0.064 and R_w = 0.064 and 0.081, respectively.

Introduction

The coordination chemistry of group 14 heterocarboranes has just begun to be investigated.[1] The most studied have been the *closo*-stannacarboranes of the C_2B_4 system. For example, donor–acceptor complexations between the stannacarboranes and Lewis bases such as monodentate ((ferrocenylmethyl)dimethylamine), bidentate (2,2′-bipyridine, 1,10-phenanthroline), bis(bidentate) (2,2′-bipyrimidine), and tridentate (2,2′:6′,2″-terpyridine) N-donor ligands have been accomplished and the X-ray crystal structures of the resulting complexes have been determined.[1-8] However, only the 2,2′-bipyridine complexes of both the *closo*-germa- and *closo*-plumbacarboranes have been reported very recently.[9-12] While the bipyridine is directly opposite the cage carbons and is symmetrically bonded to the apical tin in the stannacarborane system, the corresponding germacarborane and plumbacarborane analogues show unsymmetrical bipyridine bonding. In both the germa- and plumbacarborane complexes one M–N (M = Ge, Pb) bond is longer than the other, causing a severe tilt of the metal-

(1) (a) Hosmane, N. S.; Maguire, J. A. In *Advances in Boron and the Boranes*; Molecular Structure and Energetics 5; Liebman, J. F., Greenberg, A., Williams, R. E., Eds.; VCH: New York, 1988; Chapter 14, p 297. (b) Hosmane, N. S.; Maguire, J. A. *Adv. Organomet. Chem.* **1990**, *30*, 99. (c) Jutzi, P.; Galow, P.; Abu-Orabi, S.; Arif, A. M.; Cowley, A. H.; Norman, N. C. *Organometallics* **1987**, *6*, 1024.

(2) Hosmane, N. S.; Fagner, J. S.; Zhu, H.; Siriwardane, U.; Maguire, J. A.; Zhang, G.; Pinkston, B. S. *Organometallics* **1989**, *8*, 1769.

(3) Hosmane, N. S.; de Meester, P.; Maldar, N. N.; Potts, S. B.; Chu, S. S. C.; Herber, R. H. *Organometallics* **1986**, *5*, 772.

(4) Siriwardane, U.; Hosmane, N. S.; Chu, S. S. C. *Acta Crystallogr., Sect. C: Cryst. Struct. Commun.* **1987**, *C43*, 1067.

(5) Maguire, J. A.; Fagner, J. S.; Siriwardane, U.; Banewicz, J. J.; Hosmane, N. S. *Struct. Chem.*, in press.

(6) Hosmane, N. S.; Islam, M. S.; Siriwardane, U.; Maguire, J. A.; Campana, C. F. *Organometallics* **1987**, *6*, 2447.

(7) Siriwardane, U.; Hosmane, N. S. *Acta Crystallogr., Sect. C: Cryst. Struct. Commun.* **1988**, *C44*, 1572.

(8) Siriwardane, U.; Maguire, J. A.; Banewicz, J. J.; Hosmane, N. S. *Organometallics* **1989**, *8*, 2792.

(9) Hosmane, N. S.; Siriwardane, U.; Islam, M. S.; Maguire, J. A.; Chu, S. S. C. *Inorg. Chem.* **1987**, *26*, 3428.

(10) Hosmane, N. S.; Islam, M. S.; Pinkston, B. S.; Siriwardane, U.; Banewicz, J. J.; Maguire, J. A. *Organometallics* **1988**, *7*, 2340.

(11) Hosmane, N. S.; Lu, K.-J.; Zhu, H.; Siriwardane, U.; Shet, M. S.; Maguire, J. A. *Organometallics* **1990**, *9*, 808.

(12) Siriwardane, U.; Lu, K.-J.; Hosmane, N. S. *Acta Crystallogr., Sect. C: Cryst. Struct. Commun.* **1990**, *C46*, 1391.

0276-7333/90/2309-2798$02.50/0

bound 2,2′-bipyridine toward the two consecutive borons of the C_2B_3 face. The unusual tilting of the 2,2′-bipyridine ligand and the inequality in the M–N bond lengths could not be explained satisfactorily by MNDO-SCF calculations.[13] It was believed that the germa- and plumbacarboranes have a tendency to form one strong M–N bond, as these complexes appeared to be fluxional in solution, or alternatively, crystal-packing forces could be responsible for such structural anomalies found in these systems. In order to establish the structural and reactivity patterns in group 14 heterocarboranes, we have undertaken a detailed investigation of the coordination chemistry of both the *closo*-germa- and *closo*-plumbacarboranes. In this part of the study we describe, in detail, the preparation, characterization, and properties of 2,2′-bipyrimidine complexes of *C*-trimethylsilyl-substituted *closo*-germacarboranes and *closo*-plumbacarboranes. In addition, we also report the X-ray crystal structures of the donor–acceptor complexes 1-Ge(2,2′-$C_8H_6N_4$)-2,3-($SiMe_3$)$_2$-2,3-$C_2B_4H_4$ (I) and 1,1′-(2,2′-$C_8H_6N_4$)[1-Pb-2,3-($SiMe_3$)$_2$-2,3-$C_2B_4H_4$]$_2$ (IV) in detail.

Experimental Section

Materials. 2,3-Bis(trimethylsilyl)-2,3-dicarba-1-germa-*closo*-heptaborane(6), 2-(trimethylsilyl)-3-methyl-2,3-dicarba-1-germa-*closo*-heptaborane(6), and 2-(trimethylsilyl)-2,3-dicarba-1-germa-*closo*-heptaborane(6) and 2,3-bis(trimethylsilyl)-2,3-dicarba-1-plumba-*closo*-heptaborane(6), 2-(trimethylsilyl)-3-methyl-2,3-dicarba-1-plumba-*closo*-heptaborane(6), and 2-(trimethylsilyl)-2,3-dicarba-1-plumba-*closo*-heptaborane(6) were prepared by the methods of Hosmane et al.[10,11,14] Prior to use, 2,2′-bipyrimidine (Lancaster Syntheses, Windham, NH) was sublimed in vacuo, and the purity was checked by IR, NMR and melting point measurements. Benzene and *n*-hexane were dried over $LiAlH_4$ and doubly distilled before use. All other solvents were dried over 4–8-Å molecular sieves (Davidson) and either saturated with dry argon or degassed before use.

Spectroscopic Procedures. Proton, boron-11, and carbon-13 pulse Fourier transform NMR spectra, at 200, 64.2, and 50.3 MHz, respectively, were recorded on an IBM-200 SY multinuclear NMR spectrometer. Infrared spectra were recorded on a Perkin-Elmer Model 283 infrared spectrometer and a Perkin-Elmer Model 1600 FT-IR spectrophotometer. Mass spectral data were obtained on a Hewlett-Packard GC/MS system, Model 5988A.

Synthetic Procedures. All experiments were carried out in Pyrex glass round-bottom flasks of 250-mL capacity, containing magnetic stirring bars and fitted with high-vacuum Teflon valves. Nonvolatile substances were manipulated in either a drybox or evacuable glovebags under an atmosphere of dry nitrogen. All known compounds among the products were identified by comparing their infrared and ^{1}H NMR spectra with those of authentic samples.

Synthesis of 1-Ge^{II}-(2,2′-$C_8H_6N_4$)-2-($SiMe_3$)-3-(R)-2,3-$C_2B_4H_4$ (R = $SiMe_3$, Me, H). A benzene solution (10–15 mL) of 1-Ge-2,3-($SiMe_3$)$_2$-2,3-$C_2B_4H_4$ (1.28 g, 4.4 mmol), 1-Ge-2-($SiMe_3$)-3-(Me)-2,3-$C_2B_4H_4$ (0.38 g, 1.64 mmol), or 1-Ge-2-($SiMe_3$)-3-(H)-2,3-$C_2B_4H_4$ (0.44 g, 2.02 mmol) was poured in vacuo into a reaction flask containing anhydrous 2,2′-bipyrimidine, $C_8H_6N_4$ (0.36 g, 2.28 mmol, 0.13 g, 0.82 mmol, or 0.17 g, 1.07 mmol), at −78 °C. When the reaction flask was warmed to 0 °C, the colorless mixture turned to clear red and the solution became turbid very slowly. This mixture was constantly stirred for 7–8 days at room temperature, during which time no gas evolution was detected. The solvent, benzene, was then removed by pumping the reaction mixture over a period of 5 h in vacuo at room temperature to collect a reddish brown gummy solid in the flask. Since the gummy solid was soluble in almost all of the commonly used organic solvents, the usual purification technique that involves the washing of the product residue with dry *n*-hexane was unsuccessful. Therefore, after removal of benzene, the reaction flask was attached to a detachable U-trap, which was maintained at 0 °C. The residue in the flask was then heated gently to 40–50 °C overnight in vacuo and pumped through the U-trap at 0 °C to collect a pale yellow liquid that was later identified as the germacarborane precursor 1-Ge-2-($SiMe_3$)-3-(R)-2,3-$C_2B_4H_4$ (0.66 g, 2.27 mmol, 0.18 g, 0.78 mmol, and 0.24 g, 1.10 mmol when R = $SiMe_3$, Me, and H, respectively). No unreacted 2,2′-bipyrimidine was identified in the U-trap. After removal of all the unreacted germacarborane precursor, the reaction flask was attached to a new U-trap that was immersed in an ice bath at 0 °C. When the brownish residue was heated to 140–150 °C in vacuo, over a period of 18 h, the red crystalline solid of 1-Ge-(2,2′-$C_8H_6N_4$)-2,3-($SiMe_3$)$_2$-2,3-$C_2B_4H_4$ (I; 0.78 g, 1.74 mmol; 82% yield based on the corresponding germacarborane consumed), the orange crystalline solid of 1-Ge-(2,2′-$C_8H_6N_4$)-2-($SiMe_3$)-3-(Me)-2,3-$C_2B_4H_4$ (II; 0.26 g, 0.67 mmol; 78% yield based on the corresponding germacarborane consumed), or the red crystalline solid of 1-Ge-(2,2′-$C_8H_6N_4$)-2-($SiMe_3$)-3-(H)-2,3-$C_2B_4H_4$ (III; 0.29 g, 0.77 mmol; 84% yield based on the corresponding germacarborane consumed) was collected on the inside walls of the U-trap. The side arms of both the reaction flask and the U-trap were maintained at 140–150 °C with heating tape during the sublimation. The decomposition product elemental germanium (Ge^0) and 2,2′-bipyrimidine were not detected among the sublimates.

The physical properties and characterization of I are as follows: mp 201–203 °C; sensitive to air and moisture; moderately soluble in nonpolar organic solvents; ^{1}H NMR (C_6D_6, relative to external Me_4Si) δ 8.41 [d, 4 H, bpmd ring, $^3J(^1H–^1H)$ = 4.89 Hz], 6.32 [t, 2 H, bpmd ring, $^3J(^1H–^1H)$ = 4.88 Hz], 5.51 [q (br), 3 H, basal H_t, $^1J(^1H–^{11}B)$ = 141 Hz], 3.95 [q (br), 1 H, apical H_t, $^1J(^1H–^{11}B)$ = 160 Hz], 0.45 [s, 18 H, $SiMe_3$]; ^{11}B NMR (C_6D_6, relative to external BF_3·OEt_2) δ 23.52 [d (br), 3 B, basal BH, $^1J(^{11}B–^1H)$ = 141 Hz], −4.34 [d (br), 1 B, apical BH, $^1J(^{11}B–^1H)$ = 158 Hz]; ^{13}C NMR (C_6D_6, relative to external Me_4Si) δ 162.65 [s, 2 C, bpmd ring, NCN], 157.03 [d, 4 CH, bpmd ring, $^1J(^{13}C–^1H)$ = 182 Hz], 135.28 [s (br), cage carbon (SiCB)], 121.17 [d, 2 CH, bpmd ring, $^1J(^{13}C–^1H)$ = 170 Hz], 1.72 [q (br), 6 C, $SiMe_3$, $^1J(^{13}C–^1H)$ = 120 Hz]. The IR spectral data of I are summarized in Supplementary Table 1.

The physical properties and characterization of II are as follows: mp 218–219 °C; sensitive to air and moisture; moderately soluble in nonpolar organic solvents; ^{1}H NMR ($CDCl_3$, relative to external Me_4Si) δ 8.96 [d, 4 H, bpmd ring, $^3J(^1H–^1H)$ = 4.03 Hz], 7.39 [t, 2 H, bpmd ring, $^3J(^1H–^1H)$ = 4.02 Hz], 4.90 [q (br), 3 H, basal H_t, $^1J(^1H–^{11}B)$ = 140 Hz], 3.51 [q (br), 1 H, apical H_t, $^1J(^1H–^{11}B)$ = 162 Hz], 2.64 [s (br), 3 H, C(cage)–Me], 0.32 [s, 9 H, $SiMe_3$]; ^{11}B NMR ($CDCl_3$, relative to external BF_3·OEt_2) δ 19.84 [d (br), 3 B, basal BH, $^1J(^{11}B–^1H)$ = 139.5 Hz], −0.64 [d (br), 1 B, apical BH, $^1J(^{11}B–^1H)$ = 161.8 Hz]; ^{13}C NMR ($CDCl_3$, relative to external Me_4Si) δ 162.77 [s, 2 C, bpmd ring, NCN], 156.98 [d, 4 CH, bpmd ring, $^1J(^{13}C–^1H)$ = 184 Hz], 134.96 [s (br), cage carbon (SiCB)], 129.63 [s (br), cage carbon (CCB)], 123.65 [d, 2 CH, bpmd ring, $^1J(^{13}C–^1H)$ = 173 Hz], 22.58 [q, 1 C, C(cage)–Me, $^1J(^{13}C–^1H)$ = 125 Hz], 0.35 [q, 3 C, $SiMe_3$, $^1J(^{13}C–^1H)$ = 119 Hz]. The IR spectral data of II are summarized in Supplementary Table 1.

The physical properties and characterization of III are as follows: mp 154–156 °C; sensitive to air and moisture; moderately soluble in nonpolar organic solvents; ^{1}H NMR (C_6D_6, relative to external Me_4Si) δ 8.40 [d, 4 H, bpmd ring, $^3J(^1H–^1H)$ = 4.4 Hz], 7.29 [t, 2 H, bpmd ring, $^3J(^1H–^1H)$ = 4.4 Hz], 6.41 [s (br), 1 H, cage CH], 4.98 [q (br), 1 H, basal H_t, $^1J(^1H–^{11}B)$ = 149 Hz], 4.22 [q (br), 1 H, basal H_t, $^1J(^1H–^{11}B)$ = 142 Hz], 3.26 [q (br), 1 H, basal H_t, $^1J(^1H–^{11}B)$ = 141 Hz], 251 [q (br), 1 H, apical H_t, $^1J(^1H–^{11}B)$ = 159 Hz], 0.17 [s, 9 H, $SiMe_3$]; ^{11}B NMR (C_6D_6, relative to external BF_3·OEt_2) δ 17.9 [d (br), 1 B, basal BH, $^1J(^{11}B–^1H)$ = 150 Hz], 14.1 [d (br), 1 B, basal BH, $^1J(^{11}B–^1H)$ = 142 Hz], 7.40 [d (br), 1 B, basal BH, $^1J(^{11}B–^1H)$ = 142 Hz], −10.29 [d (br), 1 B, apical BH, $^1J(^{11}B–^1H)$ = 160 Hz]; ^{13}C NMR (C_6D_6, relative to external Me_4Si) δ 163.75 [s, 2 C, bpmd ring, NCN], 157.48 [d, 4 CH, bpmd ring, $^1J(^{13}C–^1H)$ = 184.3 Hz], 136.18 [s (br), cage carbon (SiCB)], 134.52 [d, cage CH, $^1J(^{13}C–^1H)$ = 170.3 Hz], 120.9 [d, 2 CH, bpmd ring, $^1J(^{13}C–^1H)$ = 170 Hz], −0.66 [q, 3 C, $SiMe_3$, $^1J(^{13}C–^1H)$ = 120 Hz]. The IR spectral data of III are summarized in Supplementary Table 1.

(13) Maguire, J. A.; Ford, G. P.; Hosmane, N. S. *Inorg. Chem.* **1988**, *27*, 3354.

(14) Hosmane, N. S.; Siriwardane, U.; Zhu, H.; Zhang, G.; Maguire, J. A. *Organometallics* **1989**, *8*, 566.

Synthesis of 1,1′-(2,2′-$C_8H_6N_4$)[*closo*-1-Pb-2-($SiMe_3$)-3-(R)-2,3-$C_2B_4H_4$]$_2$ (R = $SiMe_3$, Me, H). In a procedure identical with that employed in the synthesis of donor–acceptor complexes involving 2,2′-bipyrimidine and *closo*-stannacarboranes, described elsewhere,[2,6] 2.26 mmol (0.96 g) of *closo*-1-Pb-2,3-($SiMe_3$)$_2$-2,3-$C_2B_4H_4$, 2.21 mmol (0.81 g) of *closo*-1-Pb-2-($SiMe_3$)-3-(Me)-2,3-$C_2B_4H_4$, or 1.87 mmol (0.66 g) of *closo*-1-Pb-2-($SiMe_3$)-3-(H)-2,3-$C_2B_4H_4$ was reacted with freshly sublimed, anhydrous 2,2′-bipyrimidine, $C_8H_6N_4$ (0.18 g, 1.14 mmol, 0.18 g, 1.14 mmol, or 0.15 g, 0.95 mmol), in dry benzene over a period of 4 days to isolate orange, crystalline solid 1,1′-(2,2′-$C_8H_6N_4$)[*closo*-1-Pb-2,3-($SiMe_3$)$_2$-2,3-$C_2B_4H_4$]$_2$ (IV; 0.65 g, 0.65 mmol; 57% yield), pale orange crystalline solid 1,1′-(2,2′-$C_8H_6N_4$)[*closo*-1-Pb-2-($SiMe_3$)-3-(Me)-2,3-$C_2B_4H_4$]$_2$ (V; 0.57 g, 0.64 mmol; 58% yield), or orange-red solid 1,1′-(2,2′-$C_8H_6N_4$)[*closo*-1-Pb-2-($SiMe_3$)-3-(H)-2,3-$C_2B_4H_4$]$_2$ (VI; 0.39 g, 0.45 mmol; 48% yield) as the only sublimed reaction product on the inside walls of the detachable U-trap. The side arms of both the reaction flask and the U-trap were maintained at 140–150 °C with heating tape during the sublimation. A small quantity of unreacted 2,2′-bipyrimidine (0.071 g, 0.069 g, and 0.074 g when R = $SiMe_3$, Me, and H, respectively) was also recovered in a trap held at −196 °C during the mild sublimation of the dark brown reaction residue. The plumbacarborane precursors and their product of decomposition, elemental lead (Pb^0), were not identified in the sublimate. A substantial quantity of a dark brown residue that remained in the reaction flask after sublimation was discarded because of its insolubility in organic solvents. Since the complexes IV, V, and VI are not soluble in *n*-hexane at room temperature, they were washed with dry *n*-hexane in vacuo 2–3 times, vacuum-dried, and then recrystallized in hot benzene.

The physical properties and characterization of IV are as follows: mp 195–197 °C; moderately sensitive to air and moisture; slightly soluble in $CDCl_3$, C_6D_6, and THF, with the solubility increasing at higher temperature without decomposition; ^{1}H NMR ($CDCl_3$, relative to external Me_4Si) δ 9.08 [d, 2 H, bpmd ring, $^3J(^1H-^1H)$ = 4.89 Hz], 7.59 [t, 1 H, bpmd ring, $^3J(^1H-^1H)$ = 4.88 Hz], 5.56 [q (br), 1 H, basal H_t, $^1J(^1H-^{11}B)$ = 141 Hz], 4.29 [q (br), 2 H, basal H_t, $^1J(^1H-^{11}B)$ = 145 Hz], 3.16 [q (br), 1 H, apical H_t, $^1J(^1H-^{11}B)$ = 157 Hz], 0.36 [s, 18 H, $SiMe_3$]; ^{11}B NMR ($CDCl_3$, relative to external BF_3·OEt_2) δ 34.27 [d (br), 1 B, basal BH, $^1J(^{11}B-^1H)$ = 140 Hz], 27.40 [d (br), 2 B, basal BH, $^1J(^{11}B-^1H)$ = 145 Hz], −4.15 [d (br), 1 B, apical BH, $^1J(^{11}B-^1H)$ = 157 Hz]; ^{13}C NMR ($CDCl_3$, relative to external Me_4Si) 160.33 [s, 1 C, bpmd ring, NCN], 158.02 [d, 2 CH, bpmd ring, $^1J(^{13}C-^1H)$ = 186 Hz], 129.46 [s (br), cage carbons (SiCB)], 122.7 [d, 1 CH, bpmd ring, $^1J(^{13}C-^1H)$ = 171 Hz], 3.03 [q (br), $SiMe_3$, $^1J(^{13}C-^1H)$ = 119.4 Hz]. The IR spectral data of IV are summarized in Supplementary Table 1.

The physical properties and characterization of V are as follows: mp 211–212 °C; moderately sensitive to air and moisture; slightly soluble in THF, $CDCl_3$, C_6D_6, CCl_4, and CH_2Cl_2, the solubility increasing at higher temperature without any decomposition; ^{1}H NMR ($CDCl_3$ relative to external Me_4Si) δ 9.28 [d, 2 H, bpmd ring, $^3J(^1H-^1H)$ = 4.88 Hz], 7.59 [t, 1 H, bpmd ring, $^3J(^1H-^1H)$ = 4.9 Hz], 5.75 [q (br), 1 H, basal H_t, $^1J(^1H-^{11}B)$ = 153 Hz], 5.5 [q (br), 1 H, basal H_t, $^1J(^1H-^{11}B)$ = 149 Hz], 5.0 [q (br), 1 H, basal H_t, $^1J(^1H-^{11}B)$ = 150 Hz], 3.08 [q (br), 1 H, apical H_t, $^1J(^1H-^{11}B)$ = 154 Hz], 2.92 [s, 3 H, C(cage)–Me], 0.59 [s, 9 H, $SiMe_3$]; ^{11}B NMR ($CDCl_3$, relative to external BF_3·OEt_2) δ 36.36 [d (br), 1 B, basal BH, $^1J(^{11}B-^1H)$ = 153 Hz], 25.74 [d (br), 1 B, basal BH, $^1J(^{11}B-^1H)$ = 150 Hz], 24.01 [d (br), 1 B, basal BH, $^1J(^{11}B-^1H)$ = 151 Hz], −1.89 [d (br), 1 B, apical BH, $^1J(^{11}B-^1H)$ = 154 Hz]. ^{13}C NMR ($CDCl_3$, relative to external Me_4Si) δ 162.72 [s, 1 C, bpmd ring, NCN], 157.72 [d, 2 CH, bpmd ring, $^1J(^{13}C-^1H)$ = 183 Hz], 133.3 [s (br), cage carbon (SiCB)], 128.32 [s (br), cage carbon (CCB)], 121.80 [d, 1 CH, bpmd ring, $^1J(^{13}C-^1H)$ = 172 Hz], 22.74 [q, 1 C, C(cage)–Me, $^1J(^{13}C-^1H)$ = 126 Hz], 0.64 [q, 3 C, $SiMe_3$, $^1J(^{13}C-^1H)$ = 118 Hz]. The IR spectral data of V are summarized in Supplementary Table 1.

The physical properties and characterization of VI are as follows: mp 204–206 °C; moderately sensitive to air and moisture; slightly soluble in THF, $CDCl_3$, C_6D_6, CCl_4, and CH_2Cl_2, the solubility increasing at higher temperature without any decomposition; ^{1}H NMR ($CDCl_3$, relative to external Me_4Si) δ 9.06 [d, 2 H, bpmd ring, $^3J(^1H-^1H)$ = 4.86 Hz], 7.63 [t, 1 H, bpmd ring, $^3J(^1H-^1H)$ = 4.86 Hz], 6.40 [s (br), 1 H, cage CH], 5.40 [q (br), 1 H, basal H_t, $^1J(^1H-^{11}B)$ = 136 Hz], 4.10 [q (br), 1 H, basal H_t, $^1J(^1H-^{11}B)$ = 135 Hz], 3.95 [q (br), 1 H, basal H_t, $^1J(^1H-^{11}B)$ = 135 Hz], 2.75 [q (br), 1 H, apical H_t, $^1J(^1H-^{11}B)$ = 150 Hz], 0.22 [s, 9 H, $SiMe_3$]; ^{11}B NMR ($CDCl_3$, relative to external BF_3·OEt_2) δ 36.71 [d (br), 1 B, basal BH, $^1J(^{11}B-^1H)$ = 137 Hz], 24.18 [d (br), 1 B, basal BH, $^1J(^{11}B-^1H)$ = 136 Hz], 22.20 [d (br), 1 B, basal BH, $^1J(^{11}B-^1H)$ = 135 Hz], −7.33 [d (br), 1 B, apical BH, $^1J(^{11}B-^1H)$ = 151 Hz]; ^{13}C NMR ($CDCl_3$, relative to external Me_4Si) δ 161.53 [s, 1 C, bpmd ring, NCN], 157.97 [d, 2 CH, bpmd ring, $^1J(^{13}C-^1H)$ = 184 Hz], 133.0 [s (br), 1 C, cage carbon (SiCB)], 128.27 [d, C(cage)–H, $^1J(^{13}C-^1H)$ = 158 Hz], 122.48 [d, 1 CH, bpmd ring, $^1J(^{13}C-^1H)$ = 170 Hz], −0.86 [q, 3 C, $SiMe_3$, $^1J(^{13}C-^1H)$ = 119 Hz]. The IR spectral data of VI are summarized in Supplementary Table 1.

X-ray Analyses of 1-Ge(2,2′-$C_8H_6N_4$)-2,3-($SiMe_3$)$_2$-2,3-$C_2B_4H_4$ (I) and 1,1′-(2,2′-$C_8H_6N_4$)[1-Pb-2,3-($SiMe_3$)$_2$-2,3-$C_2B_4H_4$]$_2$ (IV). Since the crystals of I obtained from vacuum sublimation and by recrystallization from benzene were not of X-ray quality, they were grown slowly as pale yellow crystals from a solution in benzene that contained both the complex I and 2,2′-bipyrimidine in a 1:2 ratio. However, two crystal modifications of IV were chosen for X-ray analyses. While orange crystals of IVA were grown from benzene solution, pale yellow crystals of IVB were sublimed in vacuo onto a glass surface. The crystals all turned opaque white even upon brief exposure to air and/or moisture. Therefore, both I and IVA,B were introduced in 0.5-mm Lindemann glass capillaries in a drybox and sealed. Data were collected on an automatic Nicolet R3m/V diffractometer with Mo Kα radiation at 253 K. The pertinent crystallographic data are summarized in Table I. Three standard reflections were remeasured after every 100 reflections during the data collection. These data were corrected for decay, Lorentz–polarization effects, and absorption (based on ψ scans). The structures were solved by SHELXTL-PLUS[15] and subsequent difference Fourier maps. The cage hydrogen atoms of IVA were located in difference Fourier maps. All hydrogen atoms in both I and IVA,B were placed in calculated positions and were included in the refinement with fixed isotropic thermal parameters. Final full-matrix least-squares refinements were carried out with the SHELXTL-PLUS system of programs.[15] The function minimized was $\sum w(|F_o| - |F_c|)^2$. All non-hydrogen atoms of I and IVA,B were refined anisotropically. In the final stages of refinement a weighting scheme was used (see Table I). Scattering factors used for all atoms as well as the real and imaginary parts of the dispersion correction for Ge, Pb, and Si were those stored in SHELXTL-PLUS. The final atomic coordinates are given in Table II. Selected bond lengths, bond angles, and torsion angles are presented in Table III. The mean deviations and dihedral angles of the least-squares planes are given in Table IV.

Results and Discussion

Synthesis. In contrast to the stannacarborane system,[2,6] the *closo*-germacarboranes and *closo*-plumbacarboranes do not readily form donor–acceptor complexes with 2,2′-bipyrimidine in benzene. In fact, the benzene solution containing both the reactants had to be stirred for 4–7 days at room temperature to complete the complexation. The most interesting result was the formation of the unbridged germacarborane complexes 1-Ge(2,2′-$C_8H_6N_4$)-2,3-($SiMe_3$)$_2$-2,3-$C_2B_4H_4$ (I), 1-Ge(2,2′-$C_8H_6N_4$)-2-($SiMe_3$)-3-(Me)-2,3-$C_2B_4H_4$ (II), and 1-Ge(2,2′-$C_8H_6N_4$)-2-($SiMe_3$)-3-(H)-2,3-$C_2B_4H_4$ (III) even when the germacarborane and 2,2′-bipyrimidine were mixed in a 2:1 ratio, respectively. Perhaps this may be due to two different kinetic processes that are taking place during the complexation between the Lewis base and the germacarboranes. The slow formation of the complex, followed by a rapid intra- or intermolecular process, might have caused all the boron resonances to be

(15) Sheldrick, G. M. Structure Determination Software Programs; Nicolet Instrument Corp.: Madison, WI, 1988.
(16) This work.

Table I. Crystallographic Data[a] for I, IVA, and IVB

	I	IVA	IVB
formula	$C_{16}H_{28}B_4N_4Si_2Ge \cdot {}^1/_2C_8H_6N_4$	$C_{24}H_{50}B_8N_4Si_4Pb_2$	$C_{24}H_{50}B_8N_4Si_4Pb_2$
fw	527.5	1007.9	1007.9
cryst syst	monoclinic	monoclinic	monoclinic
space group	$P2_1/n$	$P2_1/n$	$P2_1/a$
a, Å	7.765 (9)	8.488 (5)	13.882 (5)
b, Å	37.69 (6)	24.46 (2)	9.854 (3)
c, Å	9.651 (16)	9.540 (7)	16.104 (8)
β, deg	101.41 (1)	96.20 (5)	105.91 (4)
V, Å^3	2768 (2)	1969 (2)	2118.4 (15)
Z	4	2	2
D_{calcd}, g cm^{-3}	1.266	1.70	1.580
cryst dimers, mm	0.20 × 0.20 × 0.60	0.10 × 0.20 × 0.20	0.10 × 0.40 × 0.36
scan type	$\theta/2\theta$	$\theta/2\theta$	$\theta/2\theta$
scan speed in ω: min, max, deg min^{-1}	3.5, 15.0	3.5, 15.0	3.5, 15.0
2θ range, deg	3.0, 45.0	3.0, 50.0	3.0, 50.0
no. of data collected	3967	3801	4134
T, K	253	253	253
decay, %	0	5	5
no. of unique data	3639	3485	3741
no. of obsd reflns, $I > 3.0\sigma(I)$	1654	2460	3741
R[b]	0.065	0.037	0.064
R_w	0.077	0.064	0.081
max, min $\Delta\rho$, e/Å^3	0.46, −0.44	0.85, −1.25	0.018, −0.011
k[c]	0.0009	0.0069	0.0034

[a] Graphite-monochromatized Mo Kα radiation, λ = 0.710 73 Å. [b] $R = \sum||F_o| - |F_c||/\sum|F_o|$, $R_w = [\sum w(F_o - F_c)^2/\sum w(F_o)^2]^{1/2}$. [c] $w = 1/[\sigma^2(F_o) + k(F_o)^2]$.

Table II. Atomic Coordinates (×10^4) and Equivalent Isotropic Displacement Coefficients (Å^2 × 10^3)

	x	y	z	U(eq)[a]		x	y	z	U(eq)[a]
				Compound I					
Ge	7006 (2)	1229 (1)	9481 (2)	62 (1)	C(5)	3402 (20)	881 (4)	4608 (15)	68 (7)
Si(1)	9730 (6)	1902 (1)	12351 (4)	70 (2)	C(6)	4324 (15)	796 (3)	6951 (12)	35 (5)
Si(2)	11056 (5)	1838 (1)	8717 (3)	60 (2)	C(7)	4054 (16)	627 (4)	8256 (13)	49 (5)
N(1)	5738 (13)	980 (3)	7008 (11)	58 (5)	C(8)	2617 (16)	255 (4)	9437 (16)	69 (7)
N(2)	3088 (13)	733 (3)	5778 (11)	55 (4)	C(9)	3781 (19)	341 (4)	10699 (14)	64 (6)
N(3)	2760 (14)	401 (3)	8222 (11)	56 (5)	C(10)	5029 (17)	585 (4)	10635 (14)	63 (6)
N(4)	5201 (12)	737 (3)	9419 (11)	49 (4)	C(11)	9312 (18)	2129 (4)	7777 (14)	100 (8)
N(5)	6830 (15)	97 (3)	6409 (10)	69 (5)	C(12)	12877 (19)	2090 (4)	9858 (15)	105 (8)
N(6)	6390 (13)	218 (3)	3991 (11)	57 (5)	C(13)	12117 (19)	1622 (4)	7394 (13)	87 (7)
B(3)	9745 (21)	1127 (4)	9082 (16)	65 (7)	C(14)	8114 (21)	1832 (5)	13495 (14)	119 (9)
B(4)	9192 (19)	876 (4)	10349 (18)	61 (7)	C(15)	9074 (21)	2330 (4)	11476 (14)	127 (10)
B(5)	9036 (22)	1161 (5)	11592 (18)	81 (9)	C(16)	11968 (19)	1928 (4)	13480 (14)	108 (8)
B(6)	10871 (17)	1169 (3)	10884 (14)	43 (5)	C(17)	5886 (13)	82 (3)	5100 (14)	45 (5)
C(1)	9584 (15)	1524 (3)	11101 (11)	49 (5)	C(18)	8417 (19)	247 (4)	6575 (16)	75 (7)
C(2)	10001 (15)	1511 (3)	9683 (11)	43 (5)	C(19)	9052 (18)	383 (4)	5513 (17)	76 (7)
C(3)	6000 (18)	1134 (4)	5839 (17)	75 (7)	C(20)	7965 (20)	367 (4)	4218 (16)	73 (7)
C(4)	4882 (22)	1079 (4)	4575 (15)	80 (7)					
				Compound IVA					
Pb	9159 (1)	−590 (1)	13248 (1)	40 (1)	C(3)	11357 (13)	−2196 (5)	15198 (16)	66 (5)
Si(1)	9451 (3)	−2014 (1)	15792 (3)	44 (1)	C(4)	9936 (17)	−1684 (5)	17518 (13)	68 (5)
Si(2)	5902 (3)	−1054 (1)	16148 (3)	40 (1)	C(5)	8284 (14)	−2665 (5)	15868 (15)	61 (4)
N(1)	10923 (10)	−561 (3)	10998 (9)	36 (3)	C(6)	3915 (14)	−761 (6)	15539 (13)	62 (5)
N(2)	11670 (9)	−68 (3)	9033 (8)	38 (3)	C(7)	5489 (15)	−1684 (5)	17161 (13)	64 (5)
C(1)	8378 (12)	−1540 (4)	14465 (10)	39 (3)	C(8)	6996 (16)	−554 (4)	17340 (13)	58 (4)
C(2)	7014 (11)	−1169 (4)	14587 (10)	36 (3)	C(9)	12232 (13)	−857 (5)	10999 (11)	48 (4)
B(3)	6325 (14)	−919 (5)	13125 (13)	41 (4)	C(10)	13302 (12)	−767 (6)	10093 (11)	50 (4)
B(4)	7303 (15)	−1227 (6)	11903 (13)	51 (4)	C(11)	12994 (13)	−383 (5)	9109 (12)	52 (4)
B(5)	8722 (15)	−1594 (5)	12871 (13)	47 (4)	C(12)	10734 (10)	−175 (4)	10014 (10)	36 (3)
B(6)	6742 (14)	−1637 (5)	13243 (12)	42 (4)					
				Compound IVB					
Pb	5973 (1)	6325 (1)	3367 (1)	69 (1)	C(3)	6334 (33)	4785 (88)	946 (36)	683 (124)
Si(1)	7349 (9)	5475 (11)	1391 (6)	121 (5)	C(4)	8326 (36)	4098 (44)	1542 (30)	246 (38)
Si(2)	7248 (6)	9228 (8)	2163 (6)	90 (3)	C(5)	7547 (70)	6376 (56)	585 (42)	883 (211)
N(1)	5420 (11)	4160 (17)	4193 (12)	58 (7)	C(6)	6993 (53)	10523 (39)	2902 (32)	436 (85)
N(2)	4438 (13)	3390 (16)	5086 (12)	62 (8)	C(7)	8267 (25)	9866 (51)	1886 (37)	387 (58)
C(1)	7349 (15)	6136 (20)	2465 (13)	56 (8)	C(8)	6153 (24)	9358 (53)	1391 (32)	293 (38)
C(2)	7395 (14)	7564 (20)	2773 (15)	58 (9)	C(9)	5360 (18)	2841 (26)	3861 (18)	82 (12)
B(3)	7607 (21)	7629 (25)	3826 (23)	84 (14)	C(10)	4851 (19)	1865 (26)	4099 (19)	87 (13)
B(4)	7721 (18)	6038 (21)	4138 (16)	55 (10)	C(11)	4404 (18)	2106 (25)	4726 (17)	79 (11)
B(5)	7540 (20)	5143 (22)	3268 (21)	70 (12)	C(12)	4960 (13)	4308 (21)	4794 (14)	53 (8)
B(6)	8318 (18)	6537 (24)	3350 (19)	71 (11)					

[a] Equivalent isotropic U defined as one-third of the trace of the orthogonalized U_{ij} tensor.

Table III. Bond Lengths (Å) and Selected Bond Angles and Torsion Angles (deg)

Bond Lengths (Å)

Compound I

Ge-C2B3cent	1.964	Ge-N(1)	2.572 (11)	N(5)-C(17)	1.330 (15)	N(5)-C(18)	1.335 (19)
Ge-N(4)	2.315 (11)	Ge-B(3)	2.269 (17)	N(6)-C(17)	1.314 (18)	N(6)-C(20)	1.323 (18)
Ge-B(4)	2.189 (15)	Ge-B(5)	2.330 (16)	B(3)-B(4)	1.666 (24)	B(3)-B(6)	1.793 (19)
Ge-C(1)	2.539 (12)	Ge-C(2)	2.528 (12)	B(3)-C(2)	1.557 (19)	B(4)-B(5)	1.633 (25)
Si(1)-C(1)	1.858 (13)	Si(1)-C(14)	1.847 (17)	B(4)-B(6)	1.707 (19)	B(5)-B(6)	1.697 (24)
Si(1)-C(15)	1.843 (15)	Si(1)-C(16)	1.862 (14)	B(5)-C(1)	1.534 (24)	B(6)-C(1)	1.709 (18)
Si(2)-C(2)	1.832 (13)	Si(2)-C(11)	1.836 (14)	B(6)-C(2)	1.775 (16)	C(1)-C(2)	1.468 (16)
Si(2)-C(12)	1.870 (15)	Si(2)-C(13)	1.842 (15)	C(3)-C(4)	1.366 (20)	C(4)-C(5)	1.375 (23)
N(1)-C(3)	1.319 (20)	N(1)-C(6)	1.289 (16)	C(6)-C(7)	1.463 (18)	C(8)-C(9)	1.404 (18)
N(2)-C(5)	1.324 (19)	N(2)-C(6)	1.353 (14)	C(9)-C(10)	1.344 (20)	C(17)-C(17a)	1.485 (21)
N(3)-C(7)	1.310 (17)	N(3)-C(8)	1.320 (19)	C(18)-C(19)	1.324 (23)	C(19)-C(20)	1.365 (20)
N(4)-C(7)	1.353 (15)	N(4)-C(10)	1.335 (18)				

Compound IVA

Pb-C2B3cent	2.203	Pb-N(1)	2.748 (9)	N(2)-C(11)	1.358 (14)	N(2)-C(12)	1.318 (13)
Pb-C(1)	2.711 (10)	Pb-C(2)	2.729 (10)	N(2)-Pba	2.737 (8)	C(1)-C(2)	1.486 (14)
Pb-B(3)	2.527 (12)	Pb-B(4)	2.473 (13)	C(1)-B(5)	1.585 (16)	C(1)-B(6)	1.730 (14)
Pb-B(5)	2.503 (13)	Pb-N(2a)	2.737 (8)	C(2)-B(3)	1.576 (15)	C(2)-B(6)	1.716 (15)
Si(1)-C(1)	1.878 (10)	Si(1)-C(3)	1.827 (13)	B(3)-B(4)	1.680 (18)	B(3)-B(6)	1.792 (18)
Si(1)-C(4)	1.839 (12)	Si(1)-C(5)	1.882 (12)	B(4)-B(5)	1.694 (18)	B(4)-B(6)	1.732 (18)
Si(2)-C(2)	1.896 (10)	Si(2)-C(6)	1.867 (12)	B(5)-B(6)	1.758 (18)	C(9)-C(10)	1.338 (16)
Si(2)-C(7)	1.872 (13)	Si(2)-C(8)	1.850 (12)	C(10)-C(11)	1.334 (17)	C(12)-C(12a)	1.510 (18)
N(1)-C(9)	1.327 (14)	N(1)-C(12)	1.328 (12)				

Compound IVB

Pb-C2B3cent	2.193	Pb-N(1)	2.734 (18)	N(2)-C(11)	1.387 (30)	N(2)-C(12)	1.324 (28)
Pb-C(1)	2.704 (23)	Pb-C(2)	2.710 (23)	N(2)-Pba	2.719 (21)	C(1)-C(2)	1.487 (28)
Pb-B(3)	2.536 (27)	Pb-B(4)	2.420 (23)	C(1)-B(5)	1.585 (36)	C(1)-B(6)	1.716 (29)
Pb-B(5)	2.509 (28)	Pb-N(2a)	2.719 (21)	C(2)-B(3)	1.641 (44)	C(2)-B(6)	1.694 (30)
Si(1)-C(1)	1.849 (24)	Si(1)-C(3)	1.552 (57)	B(3)-B(4)	1.641 (33)	B(3)-B(6)	1.770 (43)
Si(1)-C(4)	1.885 (47)	Si(1)-C(5)	1.657 (73)	B(4)-B(5)	1.616 (39)	B(4)-B(l)	1.766 (42)
Si(2)-C(2)	1.894 (22)	Si(2)-C(6)	1.844 (54)	B(5)-B(6)	1.731 (34)	C(9)-C(10)	1.312 (39)
Si(2)-C(7)	1.716 (48)	Si(2)-C(8)	1.684 (36)	C(10)-C(11)	1.343 (44)	C(12)-C(12a)	1.507 (41)
N(1)-C(9)	1.399 (31)	N(1)-C(12)	1.306 (31)				

Bond Angles

Compound I

N(1)-Ge-C2B3cent	125.0	N(4)-Ge-C2B3cent	124.7	Ge-B(3)-B(6)	96.5 (9)	Ge-B(3)-C(2)	80.3 (8)
N(1)-Ge-B(3)	88.8 (5)	N(1)-Ge-B(4)	105.0 (5)	Ge-B(4)-B(3)	70.6 (8)	Ge-B(4)-B(5)	73.5 (8)
N(1)-Ge-B(5)	147.1 (5)	N(4)-Ge-B(3)	116.2 (5)	Ge-B(4)-B(6)	102.2 (8)	Ge-B(5)-B(4)	64.3 (7)
N(4)-Ge-B(4)	86.7 (5)	B(3)-Ge-B(4)	43.9 (6)	Ge-B(5)-B(6)	97.1 (9)	Ge-B(5)-C(1)	79.2 (8)
N(4)-Ge-B(5)	103.7 (5)	B(3)-Ge-B(5)	68.6 (6)	N(1)-C(6)-C(7)	117.6 (10)	N(2)-C(6)-C(7)	116.4 (10)
B(4)-Ge-B(5)	42.2 (7)	Ge-N(4)-C(7)	124.2 (9)	N(5)-C(17)-C(17a)	117.7 (15)	N(6)-C(17)-C(17a)	118.2 (13)
Ge-N(4)-C(10)	119.0 (8)	Ge-B(3)-B(4)	65.5 (8)				

Compound IVA

N(1)-Pb-C2B3cent	117.5	N(2a)-Pb-C2B3cent	113.4	B(4)-Pb-B(5)	39.8 (4)	N(1)-Pb-N(2a)	58.6 (2)
N(1)-Pb-C(1)	122.4 (3)	N(1)-Pb-C(2)	145.7 (3)	C(1)-Pb-N(2a)	142.2 (3)	C(2)-Pb-N(2a)	123.3 (3)
C(1)-Pb-C(2)	31.7 (3)	N(1)-Pb-B(3)	124.6 (3)	B(3)-Pb-N(2a)	89.3 (3)	B(4)-Pb-N(2a)	82.1 (3)
C(1)-Pb-B(3)	58.1 (3)	C(2)-Pb-B(3)	34.6 (3)	B(5)-Pb-N(2a)	116.2 (3)	Pb-N(1)-C(9)	120.8 (7)
N(1)-Pb-B(4)	88.9 (4)	C(1)-Pb-B(4)	60.7 (4)	Pb-N(1)-C(12)	122.4 (6)	C(11)-N(2)-Pba	121.1 (7)
C(2)-Pb-B(4)	59.8 (4)	B(3)-Pb-B(4)	39.2 (4)	C(12)-N(2)-Pba	123.9 (6)	Pb-B(4)-B(3)	72.1 (6)
N(1)-Pb-B(5)	89.9 (3)	C(1)-Pb-B(5)	35.1 (4)	Pb-B(4)-B(5)	71.1 (6)	Pb-B(4)-B(6)	101.1 (7)
C(2)-Pb-B(5)	57.5 (4)	B(3)-Pb-B(5)	63.6 (4)				

Compound IVB

N(1)-Pb-C2B3cent	120.0	N(2a)-Pb-C2B3cent	119.8	B(4)-Pb-B(5)	38.2 (9)	N(1)-Pb-N(2a)	58.5 (5)
N(1)-Pb-C(1)	122.9 (6)	N(1)-Pb-C(2)	148.6 (5)	C(1)-Pb-N(2a)	148.9 (5)	C(2)-Pb-N(2a)	129.3 (6)
C(1)-Pb-C(2)	31.9 (6)	N(1)-Pb-B(3)	127.1 (8)	B(3)-Pb-N(2a)	94.4 (9)	B(4)-Pb-N(2a)	88.5 (8)
C(1)-Pb-B(3)	58.9 (9)	C(2)-Pb-B(3)	36.3 (10)	B(5)-Pb-N(2a)	120.6 (8)	Pb-N(1)-C(9)	122.3 (16)
N(1)-Pb-B(4)	92.1 (6)	C(1)-Pb-B(4)	60.8 (8)	Pb-N(1)-C(12)	122.2 (13)	C(11)-N(2)-Pba	119.0 (16)
C(2)-Pb-B(4)	60.6 (7)	B(3)-Pb-B(4)	38.6 (8)	C(12)-N(2)-Pba	121.9 (14)	Pb-B(4)-B(3)	74.5 (12)
N(1)-Pb-B(5)	91.9 (7)	C(1)-Pb-B(5)	35.2 (8)	Pb-B(4)-B(5)	73.9 (12)	Pb-B(4)-B(6)	101.6 (13)
C(2)-Pb-B(5)	57.2 (7)	B(3)-Pb-B(5)	62.1 (8)				

Torsion Angles

Compound I

B(3)-Ge-N(4)-C(7)	-93.4 (1.0)	B(3)-Ge-N(4)-C(10)	99.0 (1.0)
B(4)-Ge-N(4)-C(7)	-127.0 (1.1)	B(4)-Ge-N(4)-C(10)	65.4 (1.0)
B(5)-Ge-N(4)-C(7)	-165.9 (1.1)	B(5)-Ge-N(4)-C(10)	26.4 (1.1)
N(4)-Ge-B(3)-B(4)	-52.9 (0.8)	N(4)-Ge-B(3)-B(6)	-104.4 (0.7)
N(4)-Ge-B(3)-C(2)	-166.1 (0.6)	B(4)-Ge-B(3)-B(6)	-51.6 (0.8)
B(4)-Ge-B(3)-C(2)	-113.2 (1.0)	B(5)-Ge-B(3)-B(4)	42.3 (0.8)
B(5)-Ge-B(3)-B(6)	-9.3 (0.8)	B(5)-Ge-B(3)-C(2)	-71.0 (0.8)
N(4)-Ge-B(4)-B(3)	134.2 (0.8)	N(4)-Ge-B(4)-B(5)	-114.5 (0.9)
N(4)-Ge-B(4)-B(6)	-169.0 (0.9)	B(3)-Ge-B(4)-B(5)	111.3 (1.1)
B(3)-Ge-B(4)-B(6)	56.7 (0.9)	B(5)-Ge-B(4)-B(3)	-111.3 (1.1)
B(5)-Ge-B(4)-B(6)	-54.5 (1.0)	N(4)-Ge-B(5)-B(4)	69.2 (0.9)

Table III (Continued)

	Torsion Angles		
	Compound I		
N(4)-Ge-B(5)-B(6)	123.0 (0.9)	N(4)-Ge-B(5)-C(1)	-175.6 (0.8)
B(3)-Ge-B(5)-B(4)	-43.9 (0.9)	B(3)-Ge-B(5)-B(6)	9.8 (0.8)
B(3)-Ge-B(5)-C(1)	71.2 (0.9)	B(4)-Ge-B(5)-B(6)	53.8 (1.0)
B(4)-Ge-B(5)-C(1)	115.1 (1.2)	Ge-N(4)-C(7)-N(3)	-164.6 (1.0)
Ge-N(4)-C(7)-C(6)	13.1 (1.5)	Ge-N(4)-C(10)-C(9)	168.0 (1.1)
C(18)-N(5)-C(17)-C(17a)	-179.8 (1)	C(20)-N(6)-C(17)-C(17a)	179.0 (1)
N(1)-C(6)-C(7)-N(3)	-171.3 (1.2)	N(1)-C(6)-C(7)-N(4)	10.8 (1.7)
N(2)-C(6)-C(7)-N(3)	6.0 (1.8)	N(2)-C(6)-C(7)-N(4)	-171.8 (1.1)
	Compound IVA		
C(1)-Pb-N(1)-C(9)	-46.5 (0.8)	C(1)-Pb-N(1)-C(12)	148.5 (0.7)
C(2)-Pb-N(1)-C(9)	-77.4 (0.9)	C(2)-Pb-N(1)-C(12)	117.6 (0.7)
B(3)-Pb-N(1)-C(9)	-117.6 (0.8)	B(3)-Pb-N(1)-C(12)	77.3 (0.8)
B(4)-Pb-N(1)-C(9)	-100.2 (0.8)	B(4)-Pb-N(1)-C(12)	94.7 (0.7)
B(5)-Pb-N(1)-C(9)	-60.4 (0.8)	B(5)-Pb-N(1)-C(12)	134.5 (0.7)
N(2a)-Pb-N(1)-C(9)	178.4 (0.8)	N(2a)-Pb-N(1)-C(12)	13.3 (0.6)
N(1)-Pb-B(3)-B(6)	81.6 (0.6)	N(2a)-Pb-B(3)-B(6)	131.7 (0.6)
N(1)-Pb-B(4)-B(6)	145.8 (0.7)	N(2a)-Pb-B(4)-B(6)	-155.8 (0.7)
N(1)-Pb-B(5)-B(6)	-141.6 (0.6)	N(2a)-Pb-B(5)-B(6)	-87.2 (0.6)
Pb-N(1)-C(9)-C(10)	-164.8 (0.8)	C(12)-N(1)-C(9)-C(10)	1.3 (1.5)
Pb-N(1)-C(12)-N(2)	167.9 (0.7)	Pb-N(1)-C(12)-C(12a)	-13.6 (1.4)
C(9)-N(1)-C(12)-N(2)	2.1 (1.4)	C(9)-N(1)-C(12)-C(12a)	-180 (1)
C(12)-N(2) -C(11)-C(10)	0.3 (1.5)	Pba-N(2)-C(11)-C(10)	-169.6 (0.9)
C(11)-N(2)-C(12)-N(1)	-2.8 (1.4)	C(11)-N(2)-C(12)-C(12a)	178.7 (1.0)
Pba-N(2)-C(12)-N(1)	166.7 (0.7)	Pba-N(2)-C(12)-C(12a)	-11.8 (1.4)
N(1)-C(9)-C(10)-C(11)	-3.5 (1.7)	C(9)-C(10)-C(11)-N(2)	2.7 (1.7)
	Compound IVB		
C(1)-Pb-N(1)-C(9)	-35.1 (1.6)	C(1)-Pb-N(1)-C(12)	162.4 (1.2)
C(2)-Pb-N(1)-C(9)	-63.2 (1.8)	C(2)-Pb-N(1)-C(12)	134.3 (1.5)
B(3)-Pb-N(1)-C(9)	-108.7 (1.7)	B(3)-Pb-N(1)-C(12)	88.8 (1.6)
B(4)-Pb-N(1)-C(9)	-91.1 (1.5)	B(4)-Pb-N(1)-C(12)	106.4 (1.4)
B(5)-Pb-N(1)-C(9)	-52.8 (1.5)	B(5)-Pb-N(1)-C(12)	144.7 (1.4)
N(2a)-Pb-N(1)-C(9)	-178.1 (1.6)	N(2a)-Pb-N(1)-C(12)	19.4 (1.2)
N(1)-Pb-B(3)-B(6)	84.6 (1.8)	N(2a)-Pb-B(3)-B(6)	137.8 (1.5)
N(1)-Pb-B(4)-B(6)	145.9 (1.2)	N(2a)-Pb-B(4)-B(6)	-155.7 (1.2)
N(1)-Pb-B(5)-B(6)	-147.3 (1.6)	N(2a)-Pb-B(5)-B(6)	-93.4 (1.6)
Pb-N(1)-C(9)-C(10)	-160.8 (1.8)	C(12)-N(1)-C(9)-C(10)	3.1 (3.0)
Pb-N(1)-C(12)-N(2)	161.5 (1.5)	Pb-N(1)-C(12)-C(12a)	-18.9 (2.5)
C(9)-N(1)-C(12)-N(2)	-2.4 (2.7)	C(9)-N(1)-C(12)-C(12a)	177.2 (1.9)
C(12)-N(2)-C(11)-C(10)	-2.4 (2.9)	Pba-N(2)-C(11)-C(10)	-162.1 (1.7)
C(11)-N(2)-C(12)-N(1)	2.1 (2.8)	C(11)-N(2)-C(12)-C(12a)	-177 (2)
Pba-N(2)-C(12)-N(1)	161.3 (1.4)	Pba-N(2)-C(12)-C(12a)	-18.3 (2.5)
N(1)-C(9)-C(10)-C(11)	-3.7 (3.6)	C(9)-C(10)-C(11)-N(2)	3.2 (3.5)

Table IV. Mean Deviations (Å) and Dihedral Angles (deg) of the Least-Squares Planes for I•$C_8H_6N_4$, IVA, and IVB

	mean deviation		
plane	I·$C_8H_6N_4$	IVA	IVB
1 (C_2B_3 ring)	0.018	0.032	0.008
2 (C_8N_4 bipmd ring)	0.065	0.015	0.014
3 ($C_4N(1)N(2)$ pmd ring)	0.012	0.012	0.009
4 ($C_4N(3$ or $1a)N(4$ or $2a)$ pmd ring)	0.011	0.012	0.009
5 (C_8N_4 cocryst bipmd ring)	0.010		
6 ($C_4N(5)N(6)$ cocryst pmd ring)	0.009		

	dihedral angle		
planes	I·$C_8H_6N_4$	IVA	IVB
1 and 2	51.7	33.4	44.2
1 and 3	55.5	33.5	44.2
1 and 4	48.1	33.5	44.2
1 and 5	60.0		
2 and 3	4.2	0.7	0.6
2 and 4	4.2	0.7	0.6
2 and 5	10.8		
3 and 4	8.4	0	0

very broad in their ^{11}B NMR spectra. This type of kinetic behavior of the germacarborane complexes in solution was also evident during the complexation with 2,2′-bipyridine.[10] On the basis of the recovery of the germacarborane precursors, the yields of the sublimed products ranged from 78 to 84%. Although the plumbacarboranes eventually produced the expected bridged complexes 1,1′-(2,2′-$C_8H_6N_4$)[*closo*-1-Pb-2,3-$(SiMe_3)_2$-2,3-$C_2B_4H_4$]$_2$ (IV), 1,1′-(2,2′-$C_8H_6N_4$)[*closo*-1-Pb-2-$(SiMe_3)$-3-(Me)-2,3-$C_2B_4H_4$]$_2$ (V), and 1,1′-(2,2′-$C_8H_6N_4$)[*closo*-1-Pb-2-$(SiMe_3)$-3-(H)-2,3-$C_2B_4H_4$]$_2$ (VI), their slow formation is consistent with that of the germacarborane system in which complexation between the heterocarborane and Lewis base was kinetically controlled.[10,11] However, the yields of these complexes ranged from 48 to 58% after sublimation. A substantial loss in yields was due to the formation of a nonsublimable and insoluble dark brown residue that remained in the flask after sublimation.

Characterization. The unbridged germacarborane–2,2′-bipyrimidine complexes I, II, and III and the bridged plumbacarborane–2,2′-bipyrimidine complexes IV, V, and VI were characterized on the basis of ^1H, ^{11}B, and ^{13}C pulse Fourier transform NMR, IR, and mass spectroscopy (Experimental Section and Supplementary Table S1). The complexes I and IV were also characterized by single-crystal X-ray analyses (Tables I–IV).

Mass Spectra. The electron-impact (EI) mass spectra of I–VI do not exhibit the parent ion groupings. In fact, the Lewis base 2,2′-bipyrimidine ion fragment with approximately 100% relative intensity and the parent and the daughter (parent minus a methyl unit) groupings of the corresponding heterocarborane precursor have been observed. This indicates that the M–N (M = Ge, Pb) bonds in these complexes are weak, and hence, these bonds

were broken during the ionization at 70 eV. In the cases of the plumbacarboranes, the strong peaks of Pb^+ ions with the local cutoff at m/z 208 were also observed. However, the most common ion fragments in all the spectra were $(^{12}CH_3)_3{}^{28}Si^+$, $^{12}C_8H_6{}^{14}N_4{}^+$, and the corresponding *closo*-heterocarborane precursor ion (parent ion minus a bipyrimidine ligand) at their respective mass-to-charge ratios.

NMR and IR Spectra. The presence of one bipyrimidine ligand and only one germacarborane unit in each of the complexes I, II, and III is substantiated by their ^1H NMR spectra, in that the ratios of integration for $C_8H_6N_4$ and Me_3Si groups are 1:3, 2:3, and 2:3, respectively. However, except for the slight change in the chemical shifts of the basal and apical BH resonances, the proton NMR spectra of the plumbacarborane complexes IV, V, and VI are identical with those of the stannacarborane analogues,[2,6] indicating that there are two plumbacarborane units and one bipyrimidine ligand in each of these complexes. In addition, the ^1H NMR spectra of all the complexes showed very broad BH resonances. The presence of C(cage)–methyl group(s) in II and V and C(cage)–H group(s) in III and VI was also evident in their ^1H NMR spectra (see Experimental Section). The ^{13}C NMR spectra clearly indicate the presence of a 2,2′-bipyrimidine molecule in addition to Me_3Si and Me or CH groups in I–VI. Since there are no significant changes in the ^{13}C chemical shifts of the cage carbons from those of the *closo*-germa- or *closo*-plumbacarborane precursors, it could be that the extent of the interaction between the apical heteroatom and the cage carbons remained more or less the same even after the complexation with 2,2′-bipyrimidine. However, this type of ^{13}C NMR spectral pattern has been observed for the (ferrocenylmethyl)dimethylamine,[2] 2,2′-bipyridine,[3,4] 2,2′-bipyrimidine,[2,6] 1,10-phenanthroline,[5] and 2,2′:6′,2″-terpyridine[7,8] complexes of the stannacarboranes, indicating that ^{13}C chemical shifts do not provide sufficient information regarding the cage geometries in these systems. While there are little or no changes in the chemical shifts of the basal and apical boron resonances in the ^{11}B NMR spectra of I and II from those of the heterocarborane precursors, the apical boron resonances of III are significantly shifted upfield due to interaction of Ge with the N-donor atom(s) of the 2,2′-bipyrimidine ligand, consistent with the interpretation that the Ge–N bonds in III are stronger than those in I and II. However, the structural evidence for the stronger Ge–N interaction in III could not be provided, since X-ray-quality crystals of III are not yet available. Therefore, it is premature to make any conclusions on the strength of the Ge–N bonds in III on the basis of its NMR spectral data alone. It is of interest to note that the crystal structure of I (discussed in the following section) shows that the molecule consists of one strong and one weak Ge–N bond and is consistent with its ^{11}B NMR spectrum. Since the ^{11}B NMR spectra of the plumbacarborane complexes IV–VI are unexceptional and are consistent with the crystal structure of IV, they deserve no special comment. The presence of the coordinated 2,2′-bipyrimidine ligand and the corresponding heterocarborane cages was also confirmed by the infrared spectra of I–VI (see Supplementary Table S1).

Crystal Structures of 1-Ge(2,2′-$C_8H_6N_4$)-2,3-($SiMe_3$)$_2$-2,3-$C_2B_4H_4$ (I) and 1,1′-(2,2′-$C_8H_6N_4$)[1-Pb-2,3-($SiMe_3$)$_2$-2,3-$C_2B_4H_4$]$_2$ (IV). Among the known germacarboranes of the C_2B_4 system to date, structural information is available for *commo*-1,1′-Ge^{IV}[2,3-(Me_3Si)$_2$-2,3-$C_2B_4H_4$]$_2$,[17,18] *closo*-1-Ge^{II}-2,3-($SiMe_3$)$_2$-5-($Ge^{IV}Cl_3$)-2,3-$C_2B_4H_3$,[19] and the donor–acceptor complex 1-Ge^{II}-(2,2′-$C_{10}H_8N_2$)-2,3-($SiMe_3$)$_2$-2,3-$C_2B_4H_4$.[9,10] Unlike the cases of the stannacarborane systems, it is somewhat difficult to rationalize the extent of the slip distortion in the donor–acceptor complexes of the germacarboranes since the structures of the *closo*-germacarborane precursors are still unknown. Although the slippage of the germanium away from the cage carbons and toward the ring borons is similar to that found in the structure of the bipyridine–stannacarborane complexes,[3,4] the structure of 1-Ge^{II}(2,2′-$C_{10}H_8N_2$)-2,3-($SiMe_3$)$_2$-2,3-$C_2B_4H_4$ differs significantly in that the apical germanium is twisted away from the carborane mirror plane so that the two Ge–B bond distances are unequal. Furthermore, the germanium in the complex was considered to be η^2-bonded to the unique boron and one other basal boron. The two Ge–N bonds are also nonequivalent, with one bond distance being 0.15 Å longer than the other.[9,10] In the present study, the structural investigation of the bipyrimidine complexes of the *closo*-germacarborane (I) was undertaken in order to establish the structural pattern in these systems. The crystal structure of I is consistent with the NMR spectra and shows that the complex consists of only one distorted germacarborane unit and the apical germanium is bonded to a bipyrimidine ligand. Figure 1 shows the thermal ellipsoid diagram of the complex I with the solvated bipyrimidine. Since the crystals of the complex were grown from the benzene solution containing excess bipyrimidine, the presence of one solvated bipyrimidine molecule in the crystal lattice is not surprising. The closest contacts of the atoms of the free 2,2′-bipyrimidine with the atoms of I are those between C(17) and N(2) in one molecule and C(19) and N(2) in the other with distances of 3.427 and 3.361 Å, respectively. However, these nonbonded contacts exceed the sum of their van der Waals radii. Therefore, the presence of this solvated bipyrimidine does not affect the geometry of the complex I. The structure reveals that the Ge atom is slip-distorted as indicated by the longer Ge–C

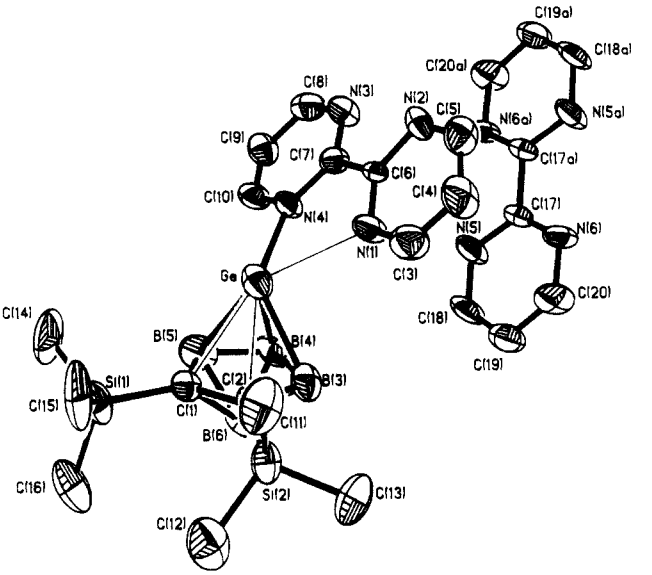

Figure 1. Perspective view of 1-Ge(2,2′-$C_8H_6N_4$)-2,3-($SiMe_3$)$_2$-2,3-$C_2B_4H_4$ (I), with the cocrystallized 2,2′-bipyrimidine in the unit cell. The thermal ellipsoids are drawn at the 30% probability level, showing the atom-numbering scheme.

(17) Hosmane, N. S.; de Meester, P.; Siriwardane, U.; Islam, M. S.; Chu, S. S. C. *J. Am. Chem. Soc.* **1986**, *108*, 6050.

(18) Islam, M. S.; Siriwardane, U.; Hosmane, N. S.; Maguire, J. A.; de Meester, P.; Chu, S. S. C. *Organometallics* **1987**, *6*, 1936.

(19) Siriwardane, U.; Islam, M. S.; Maguire, J. A.; Hosmane, N. S. *Organometallics* **1988**, *7*, 1893.

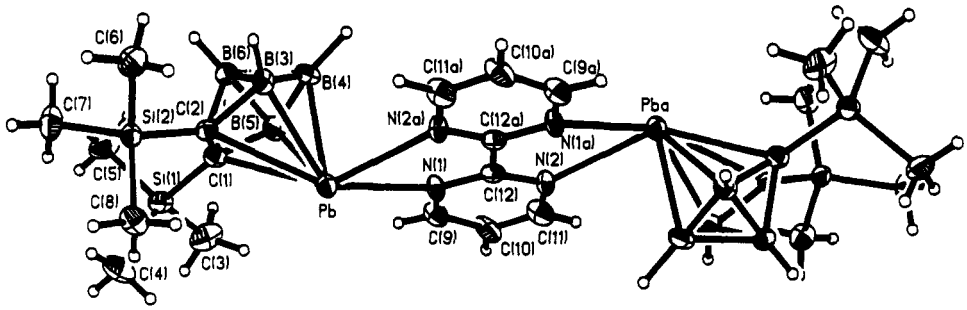

Figure 2. Perspective view of 1,1′-(2,2′-$C_8H_6N_4$)[1-Pb-2,3-($SiMe_3$)$_2$-2,3-$C_2B_4H_4$]$_2$ (IVA) showing the trans configuration of the plumbacarboranes with the atom-numbering scheme and thermal ellipsoids at the 30% probability level. The midpoint of the C(12)–C(12a) bond lies at the center of symmetry.

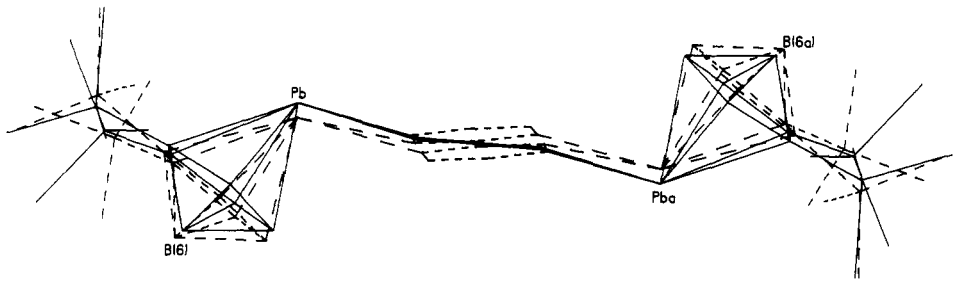

Figure 3. Superimposed line drawings of the two crystal modifications of IV. The unbroken and broken line drawings represent the structures of IVA and IVB, respectively.

distances compared to those of Ge–B (see Table III). The distance of the germanium from the center of the C_2B_3 face is 1.964 Å. Although the apical Ge is η^3-bonded to the cage borons, most of the Ge–cage bond distances in I are similar to those found in the structure of 1-Ge^{II}(2,2′-$C_{10}H_8N_2$)-2,3-($SiMe_3$)$_2$-2,3-$C_2B_4H_4$.[9,10] However, there are several interesting features in the structure of I. Apart from the overall nonplanarity of the Ge-bound 2,2-bipyrimidine compared to the cocrystallized free 2,2′-bipyrimidine (see Table IV), the base is tilted significantly away from the cage carbons with B–Ge–N orientation angles of about 86–147°. Consequently, the Ge–N(1) distance of 2.572 (11) Å is longer than the Ge–N(4) distance (2.315 (11) Å). The difference of about 0.25 Å between the two M–N (M = metalloid or metal) bonds in the present study is substantially greater than those of 0.15 and 0.1 Å found in the structures of 1-Ge^{II}(2,2′-$C_{10}H_8N_2$)-2,3-($SiMe_3$)$_2$-2,3-$C_2B_4H_4$,[9,10] and 1-Pb^{II}(2,2′-$C_{10}H_8N_2$)-2,3-($SiMe_3$)$_2$-2,3-$C_2B_4H_4$,[11] respectively. Perhaps unrestricted rotation of the C(6)–C(7) (see Figure 1) bond in the Lewis base and the slow rate of complexation between the Ge atom and the weaker bipyrimidine base that results in the formation of only one Ge–N bond, combined with the fluxional behavior of the heterocarorane cage, may be responsible for the formation of the unbridged 2,2′-bipyrimidine complex of the *closo*-germacarboranes. However, both the stannacarborane and plumbacarborane systems exclusively produce the bridged donor–acceptor complexes with 2,2′-bipyrimidine.[2,6,16] The dihedral angles between the planes formed by the C_2B_3 faces of the carborane and C_4N_2 rings of the coordinated bipyrimidine ligand containing N(1), N(2) and N(3), N(4) donor atoms in I are 55.5 and 48.1°, respectively, while the dihedral angle between the C_2B_3 plane and the average plane of the bipyrimidine ligand is 51.7° (see Table IV). All of these angles are substantially greater than the dihedral angles of 26.8 and 44.2° found between the C_2B_3 face and the rings of the 2,2′-bipyridine and bipyrimidine bases in the donor–acceptor complexes of *closo*-stannacarboranes, respectively.[2-4,6] The corresponding angle in 1-Ge^{II}(2,2′-$C_{10}H_8N_2$)-2,3-($SiMe_3$)$_2$-2,3-$C_2B_4H_4$[9,10] is 32.5°, which is also smaller than that found in the present system. It is apparent from Figure 1 and from Tables III and IV that the Lewis base 2,2′-bipyrimidine is not symmetrically bonded to the apical germanium in I and that the base acts as a monodentate ligand in forming the donor–acceptor complexes of the *closo*-germacarboranes.

The structures of IV have been determined for its two crystal modifications, IVA and IVB. Figure 2 represents the thermal ellipsoid diagram for IVA, while Figure 3 contains superimposed line drawings of the structures of both molecules. The calculated density of IVA is greater than that of IVB (1.70 vs 1.58 g cm^{-3}; see Table I), and these values are consistent with the packing diagrams (Figure 4), which show that the Pb atoms of the two molecules in the unit cell of the former are closer by about 4.528 Å with a Pb---C(8) nonbonded contact of about 4.343 Å; the rest of the nonbonded contacts in the former and all of the nonbonded contacts in the unit cell of the latter are greater than 5.0 Å. However, the molecular geometries of both molecules are identical within the limits of crystallographic errors of determinations (see Figures 2 and 3 and Table III). The distances between the C_2B_3 center and the apical Pb atom in IVA and IVB are 2.203 and 2.193 Å, respectively. All the distances indicate that the extent of slip distortions in both molecules is on the same order with a difference of about 0.25–0.28 Å between the average Pb–C(cage) and Pb–B(unique) bonds and is similar to the difference of about 0.266 Å found between the Sn–C(cage) and Sn–B(unique) distances in the stannacarborane analogue.[2] The Pb–N distances of 2.748 (9) and 2.737 (8) Å in molecule IVA and 2.734 (18) and 2.719 (21) Å in molecule IVB are significantly longer than those of 1-Pb^{II}(2,2′-$C_{10}H_8N_2$)-2,3-($SiMe_3$)$_2$-2,3-$C_2B_4H_4$ (2.674 (9) and 2.581 (9) Å)[11] and 1-Pb^{II}(2,2′-$C_{10}H_8N_2$)-2-($SiMe_3$)-3-(Me)-2,3-$C_2B_4H_4$ (2.615 (7) and 2.663 (7) Å),[12] indicating a weaker interaction of the 2,2′-bipyrimidine ligand with the Pb atom in IV. This is consistent with the interaction observed in the stannacarborane systems.[2-7] The bipyrimidine bases in IVA and IVB are directly opposite the cage carbons, and the dihedral angles between the pyrimidine rings and the C_2B_3 faces of the heterocarboranes

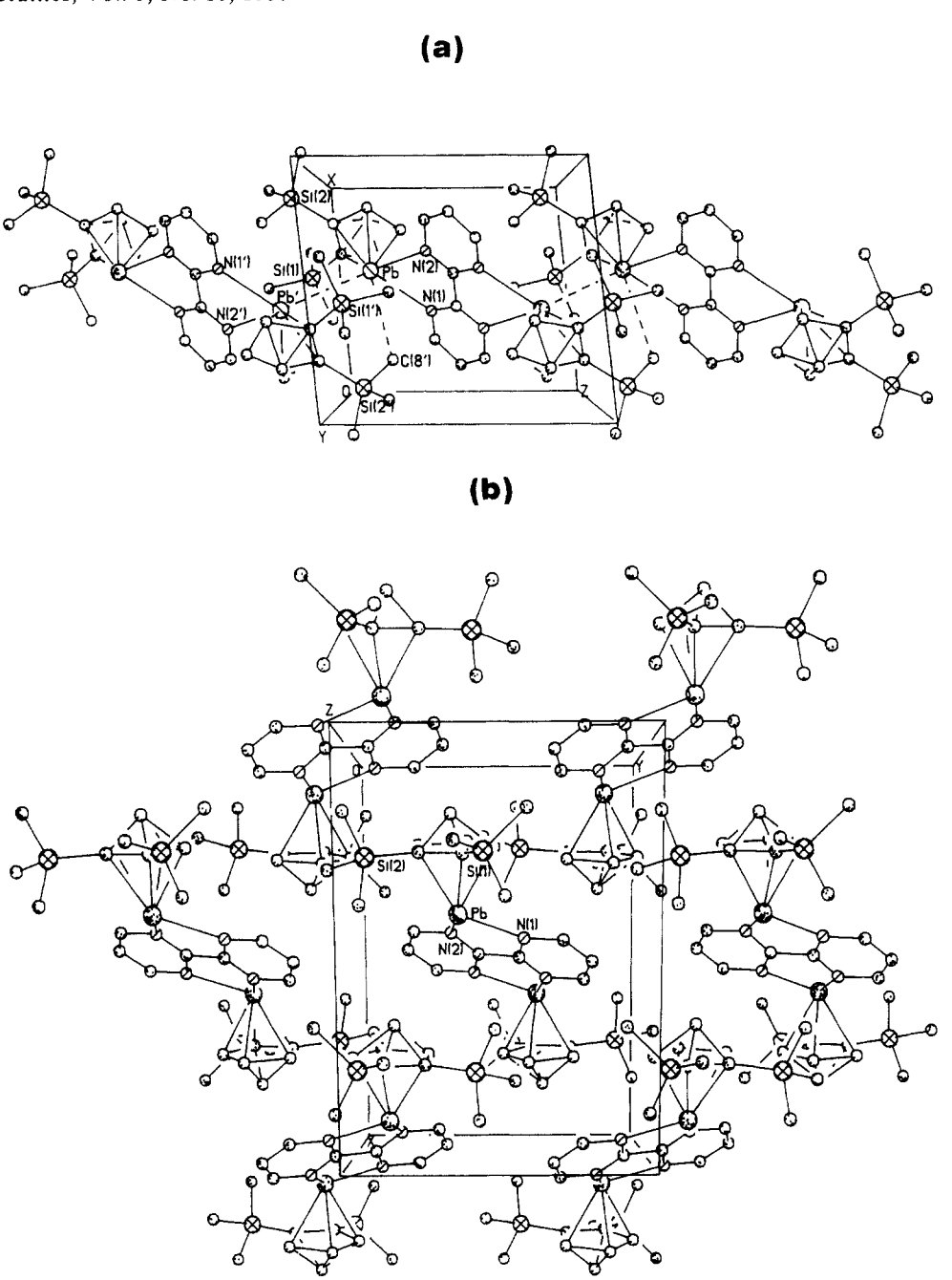

Figure 4. Crystal-packing diagrams showing the closer Pb···Pb (4.528 Å) and Pb–C(8) (4.343 Å) distances in IVA (a) than the corresponding distances of 7.596 and 9.754 Å in IVB (b).

are 33.5° in the former and 44.2° in the latter (see Table IV). It has recently been established[2,5,8,11,13] that the most efficient bonding between the heteroatom and the Lewis bases occurs when the planar bases and the C_2B_3 faces align parallel with a dihedral angle of 0°. However, repulsion between the two ligands results in slipping the apical heteroatom toward the ring borons on complexation with the Lewis base by decreasing or breaking the interaction of the heteroatom to the cage carbons and minimizing the ligand–ligand repulsion. In general, when a stronger base interacts with the heteroatom, the slippage of the heteroatom increases and, consequently, the dihedral angles between the base and the C_2B_3 faces decrease. This is precisely what has been observed in the stannacarborane,[2-8] germacarborane,[9,10,16] and plumbacarborane[11,12,16] systems; that is, adducts with monodentate Lewis bases show less slip distortion than that found in the bipyridine complexes, as does the complex with the weaker bipyrimidine base. However, the dihedral angle of 33.5° between the two ligands in IVA is substantially smaller than the 44.2° angle of IVB (see Table IV), indicating that there is a stronger interaction (though not as strong as those in the 2,2′-bipyridine complexes) between the apical Pb atom and the two N-donor atoms of the 2,2′-bipyrimidine in IVA than in IVB. In contrast, the Pb–N distances in both molecules are almost identical within the limits of crystallographic errors (see Table III). Even though there are not significant bonding differences between the two molecules, IVA is denser than IVB (1.70 vs 1.58 g cm^{-3}), indicating that there is also a direct correlation between the ligand–ligand dihedral angle and the crystal packing. Therefore, a great deal of caution should be exercised before any theoretical calculations are applied in explaining slip distortions in heterocarboranes and in attributing these distortions to internal bonding preferences. As in the case of the stannacarborane system, the trans orientations of the plumbacarboranes in IVA and IVB are favored on steric grounds.[2]

Since the stannacarborane[2,6] and the plumbacarborane systems[16] produce stable, bridged donor–acceptor com-

plexes with 2,2′-bipyrimidine, the unbridged germacarborane complexes produced in the present investigation could be complexed further with either stanna- or plumbacarboranes by utilizing the uncoordinated N-donor atoms of the Ge-bound 2,2′-bipyrimidine to produce novel, bridged heterobimetallacarborane complexes. Such an endeavor is currently underway in our laboratories.

Acknowledgment. This work was supported by grants from the National Science Foundation (Grant No. CHE-8800328), the Robert A. Welch Foundation (Grant No. N-1016), and the donors of the Petroleum Research Fund, administered by the American Chemical Society. We thank Dr. Hongming Zhang for his assistance in preparing tables of X-ray data.

Supplementary Material Available: Listings of IR absorptions (Table S-1) of I–VI and of anisotropic displacement coefficients (Table S-2), bond angles and torsion angles (Table S-3), and H atom coordinates and isotropic displacement coefficients of I, IVA, and IVB (Table S-4) (15 pages); listings of structure factors of I, IVA, and IVB (Table S-5) (34 pages). Ordering information is given on any current masthead page.

Synthesis and Characterization of Copper(I) Trifluoroacetate Alkyne Complexes of the Type $Cu_4(\mu\text{-}O_2CCF_3)_4(\mu\text{-alkyne})_2$ and $Cu_2(\mu\text{-}O_2CCF_3)_2(alkyne)_2$

Daniel L. Reger* and Mark F. Huff

Department of Chemistry, University of South Carolina, Columbia, South Carolina 29208

Received March 6, 1990

The complex $Cu_4(\mu\text{-}O_2CCF_3)_4(\mu\text{-}EtC{\equiv}CEt)_2$ (1) is prepared from 3-hexyne and $Cu_4(\mu\text{-}O_2CCF_3)_4(C_6H_6)_2$ followed by recrystallization from hexane. Recrystallization from hexane containing added 3-hexyne yields $Cu_2(\mu\text{-}O_2CCF_3)_2(EtC{\equiv}CEt)_2$ (2). Molecular weight studies show these stoichiometries are retained in solution. Low-temperature NMR spectra show that complex 2 is in equilibrium with 1 and free 3-hexyne, whereas 2 is not observed in solutions of 1. The tetranuclear complexes $Cu_4(\mu\text{-}O_2CCF_3)_4(\mu\text{-}RC{\equiv}CCO_2Me)_2$ (R = CO_2Me (3), Me (4)), analogous to 1, form in reactions of $Cu_4(\mu\text{-}O_2CCF_3)_4(C_6H_6)_2$ and $MeO_2CC{\equiv}CCO_2Me$ or $MeC{\equiv}CCO_2Me$, respectively. In contrast, only the dinuclear complex $Cu_2(\mu\text{-}O_2CCF_3)_2(PhC{\equiv}CPh)_2$ (5), analogous to 2, forms in the reaction with diphenylacetylene. Competition studies indicate that the affinity of these alkynes for copper(I) in this system is similar for 3-hexyne, $MeO_2CC{\equiv}CCO_2Me$, and $MeC{\equiv}CCO_2Me$, but diphenylacetylene has a lower affinity.

Introduction

Continuing our interest in η^2-alkyne complexes of the transition metals,[1] we have initiated an investigation of alkyne complexes of copper(I). We began our investigations with the synthesis of alkyne complexes of copper(I) trifluoroacetate because similar $[Cu(\mu\text{-}O_2CCF_3)(alkene)]_n$ complexes had been prepared previously and are quite stable.[2] Prior to our work, the only copper(I) acetate alkyne complex that had been definitively characterized was the dinuclear complex $Cu_2(\mu\text{-}O_2CPh)_2(PhC{\equiv}CPh)_2$.[3]

In our first report in this area, we communicated the synthesis and solid-state structure of the unusual tetranuclear complex $Cu_4(\mu\text{-}O_2CCF_3)_4(\mu\text{-}EtC{\equiv}CEt)_2$ (1). Complex 1 contains two alkyne ligands bridging copper atoms not directly bridged by other ligands.[4] A very recent publication has reported additional examples of the analogous tetranuclear, 2-substituted copper(I) benzoate complexes $Cu_4(\mu\text{-}O_2CC_6H_4\text{-}2\text{-}X)_4(\mu\text{-}RO_2CC{\equiv}CCO_2R)_2$ (X = H, Cl, Br; R = Me, Et).[5] We report here the synthesis of a series of alkyne complexes of copper(I) trifluoroacetate. With 3-hexyne, careful control of the purification procedures can lead to the synthesis of the dinuclear complex $Cu_2(\mu\text{-}O_2CCF_3)_2(EtC{\equiv}CEt)_2$ (2). In addition, we show that the copper to alkyne stoichiometry (either 4:2 or 2:2) can also be controlled by the choice of alkyne.

Experimental Section

General Procedure. All operations were carried out under a nitrogen atmosphere with use of either standard Schlenk techniques or a Vacuum Atmospheres HE-493 drybox. All solvents were dried, degassed, and distilled prior to use. Infrared spectra were recorded on a Perkin-Elmer 781 spectrophotometer. The ^1H and ^{13}C NMR spectra were recorded on Bruker AM-300 and AM-500 spectrometers using a 5-mm broad-band probe. Proton and carbon chemical shifts are reported in ppm downfield from TMS with use of the solvents CD_3COCD_3 (δ(H) = 2.04 ppm, δ(C) = 29.8, 206.0 ppm), C_6D_6 (δ(H) = 7.15 ppm, δ(C) = 128 ppm), and $C_6D_5CD_3$ (δ(H) = 2.09 ppm, δ(C) = 20.4 ppm) as internal standards. All spectra were recorded at room temperature unless otherwise indicated. Elemental analyses were performed by Robertson Laboratories, Inc. Mass spectra were run on a Finnigan 4521 GC–mass spectrometer. The clusters assigned to specific ions show the appropriate patterns as calculated for the atoms present. $Cu_4(\mu\text{-}O_2CCF_3)_4(C_6H_6)_2$[2a] was prepared by published methods. Molecular weights were determined by freezing point depression measurements in an apparatus similar in basic design to that described by Shriver.[6] The cell contains a Fenwal GB41P2 10-kΩ thermistor, balanced against a Leeds & Northrup bridge circuit. A working calibration curve of molality versus ΔT was obtained by using known concentrations of doubly sublimed ferrocene. Data acquisition and processing were automated by interfacing the apparatus to a WYSE 286 computer. Typically, the mass of a sample was determined on a benchtop analytical

(1) (a) Reger, D. L. *Acc. Chem. Res.* **1988**, *21*, 229. (b) Reger, D. L.; Klaeren, S. A.; Lebioda, L. *Organometallics* **1988**, *7*, 189.

(2) (a) Rodesiler, P. F.; Amma, E. L. *J. Chem. Soc., Chem. Commun.* **1974**, 599. (b) Reger, D. L.; Dukes, M. D. *J. Organomet. Chem.* **1976**, *113*, 173.

(3) Pasquali, M.; Leoni, P.; Floriani, C.; Gaetani-Manfredotti, A. *Inorg. Chem.* **1982**, *21*, 4324.

(4) Reger. D. L.; Huff, M. F.; Wolfe, T. A.; Adams, R. D. *Organometallics* **1989**, *8*, 848.

(5) Aalten, H. L.; van Koten, G.; Riethorst, E.; Stam, C. H. *Inorg. Chem.* **1989**, *28*, 4140.

(6) Shriver, D. F.; Drezdzon, M. A. *The Manipulation of Air-Sensitive Compounds*, 2nd ed.; Wiley: New York, 1986; p 38.

0276-7333/90/2309-2807$02.50/0